Location of Subunits within the Acetylcholine Receptor by Electron Image Analysis of Tubular Crystals from *Torpedo marmorata*

Elizabeth Kubalek,‡ Scott Ralston,* Jon Lindstrom,* and Nigel Unwin‡

*Salk Institute, La Jolla, California 92138; and ‡Department of Cell Biology, Stanford University Medical School, Stanford, California 94305

Abstract. The binding sites on the nicotinic acetylcholine receptor of labels specific for the α-, β-, and δ-subunits were determined by electron image analysis, using tubular crystals of receptors grown from the postsynaptic membranes of *Torpedo marmorata* electric organ. The labels were α-bungarotoxin (which attaches to the acetylcholine binding sites on the pair of α-subunits), Fab35 (a monoclonal antibody Fab fragment directed against the main immunogenic region of the α-subunit), FabIII (a monoclonal antibody Fab fragment directed against a cytoplasmic site on the β-subunit), and wheat germ agglutinin (which binds to *N*-acetylglucosamine residues on the δ-subunit). These labels, bound to receptors in the crystals, were located by comparing labeled with native structures, averaged in each case over more than 5,000 molecules.

From the assignments made, we find that the clockwise arrangement of subunits around the receptor, viewed from the synaptic face, is: α, β, α, γ, and δ; that the main immunogenic region is at (or close to) the side of the α-subunit; and that the two acetylcholine binding sites are at the synaptic end of the α-subunits, 27–28 Å from the central axis and ~53 Å apart. In the crystal lattice, neighboring molecules are paired so that their δ- and α-subunits are juxtaposed, an organization that appears to relate closely to the grouping of receptors in vivo.

THE nicotinic acetylcholine receptor is an oligomeric membrane protein composed of four different but homologous polypeptide chains: α, β, γ, and δ (for recent reviews, see references 22 and 25). It contains two copies of the α-subunit and single copies of β, γ, and δ. This five subunit assembly in the lipid bilayer forms a ring, the central axis of which delineates a gated, cation-selective channel.

Conflicting results have emerged from electron microscopic and biochemical cross-linking experiments to probe the relative locations of these subunits around the channel. The acetylcholine binding site on the α-subunit has been identified by imaging receptors labeled with cobra toxin complexed to biotin-avidin (14). By use of this label and by analysis of receptors linked together through their δ- or β-subunits, it has been deduced that the probable circular arrangement of the subunits around the channel is α, γ, α, β, and δ (17). In contrast, receptor-specific ligands modify the α-neurotoxin cross-linking pattern in a way that suggests that β, rather than γ, may lie between the two α-subunits (11). Other interpretations have also supported this latter view (8, 35).

Here we examine subunit-specific labels bound to receptors crystallized on native membrane vesicles (3) to locate binding sites and hence determine the circular arrangement of the subunits. The analysis also reveals the organization of individual receptors within the crystal lattice. Since the crystals are formed by lateral aggregation of ribbons of paired receptors (3) and such ribbons are also present on the postsynaptic membranes (13), this organization appears to relate closely to the grouping of receptors in vivo.

Materials and Methods

Materials

Wheat germ agglutinin (WGA),[1] α-bungarotoxin (BTX), and α-chloronapthol were from Sigma Chemical Co., St. Louis, MO: WGA-biotin was from E. Y. Laboratories, Inc., San Mateo, CA; avidin-peroxidase was from Vector Laboratories, Inc., Burlingame, CA; nitrocellulose was from Schleicher & Schuell, Inc., Keene, NH. Other chemicals were from standard sources and were of reagent grade.

Monoclonal antibodies 35 and III (mAb35 and mAbIII) were prepared as described (30, 31). Fab fragments of the antibodies, Fab35 and FabIII, were prepared by the standard procedures (21). Table I shows details of these and the other labeling reagents used.

Isolation and Biochemical Characterization

Crystalline vesicles of tubular morphology ("tubes") were prepared from freshly killed and dissected *Torpedo marmorata* (Marine Station, Arcachon, France) essentially as described (3) except for the addition of 1 mM *n*-ethyl-

Address correspondence to Dr. Unwin.

1. *Abbreviations used in this paper*: BTX, α-bungarotoxin; WGA, wheat germ agglutinin.

Table I. Characteristics of Labeling Reagents

Label	Specificity	M_r
BTX	α*	~8,000
Fab35	α‡	~50,000
Fab111	β§	~50,000
WGA	δ‖	~36,000

* Acetylcholine binding site; extracellular; including residues 192, 193 (16, 26, 34).
‡ Main immunogenic region; extracellular; residues 46–127 (27).
§ Cytoplasmic; residues 360–410 (27, 28).
‖ Extracellular (24).

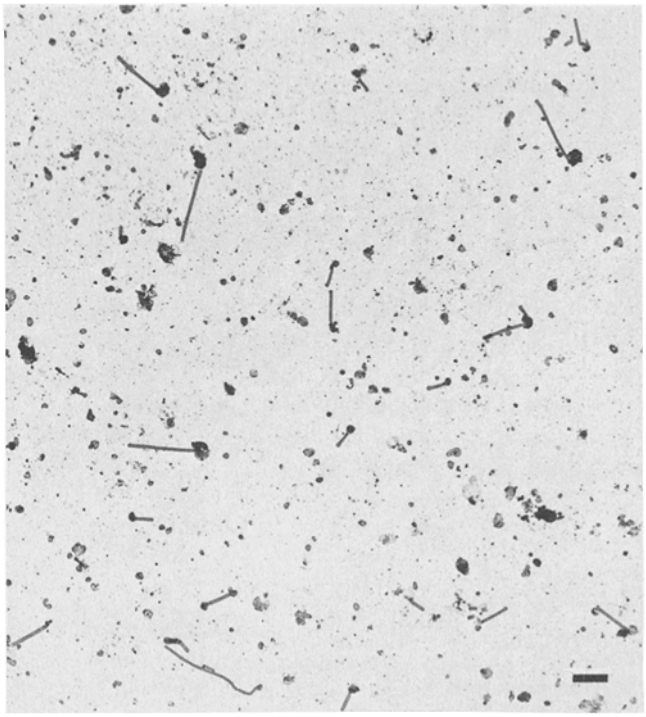

Figure 1. Sample of a membrane preparation incubated for 4 wk at 17°C, showing the typical proportion of rounded vesicles and tubes. Only about half of the rounded vesicles are rich in receptors; many of these receptors are also packed in a regular way. Bar, 1 μm.

maleimide to the isolation buffer and substitution of 100 mM sodium cacodylate, pH 6.8, and protease inhibitors (0.3 μg/ml leupeptin and 1 μg/ml pepstatin) for Tris-HCl in the final solutions. Receptors in these tubes are organized on a surface lattice with the symmetry of the plane group, p2 (approximate unit cell dimensions: a = 90 Å, b = 162 Å, and included angle γ = 117° [3]). In the best preparations, at least 10% of the receptor-rich vesicles developed into tubes after incubating at 17°C over a period of ~4 wk (Fig. 1).

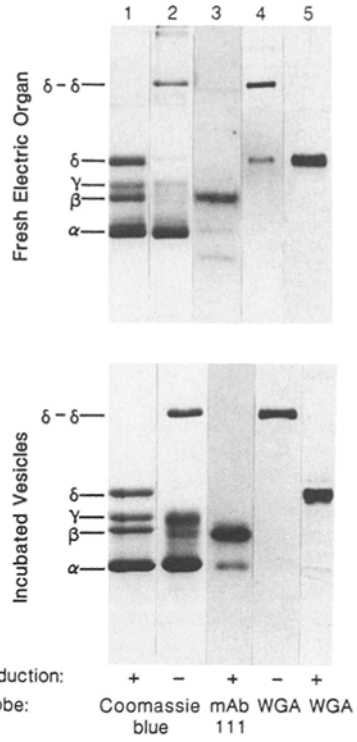

Figure 2. Biochemical characterization of purified *T. marmorata* receptor and labeling reagents. Receptors purified from fresh electric organ (*top*) or from the incubated preparation shown in Fig. 1 (*bottom*) were subjected to SDS PAGE. The samples were stained with Coomassie Blue (lanes *1* and *2*), or electro-transferred to nitrocellulose and probed with monoclonal antibody 111 (lane *3*) and WGA (lanes *4* and *5*), as described in Materials and Methods. 10 μg of receptor were subjected to electrophoresis on lanes *1* and *2*, and ~1 μg on lanes *3–5*. The samples in lanes *1*, *3*, and *5* were reduced with 2% β-mercaptoethanol before electrophoresis. The slight apparent cross-reaction of mAb111 with α-subunits of the incubated vesicles is most likely due to the presence of small amounts of a proteolytic fragment of the β-subunit, since the titer of mAb111 reacted with the α-subunit is <1% of that obtained with β (10). Extensive proteolysis of the receptor can make it appear to consist only of α-subunits (20).

Receptor was purified from these preparations and from the fresh electric organ by affinity chromatography on toxin-agarose (19). The purified material was denatured in 2% SDS in the presence and absence of 2% β-mercaptoethanol, and subjected to SDS PAGE (19). The samples on the gels were either stained with Coomassie Blue or electro-transferred to nitrocellulose or diazophenylthioether paper (27).

WGA labeling of the subunits was by the method of Nomoto et al. (24). The nitrocellulose sheet was quenched by three 10-min washes in 100 mM NaCl, 10 mM sodium phosphate, pH 7.5 (PBS) containing 0.1% Tween 20 (quench buffer). The sheet was incubated (1 h at room temperature) with WGA-biotin (5 μg/ml) in the quench buffer using a volume of ~8 ml/100

Figure 3. Steps used in processing electron micrographs: (*a*) densitometer display of a native tube (reversed contrast compared with Fig. 4), showing area (473 × 129 array size) selected for analysis; (*b*) computed diffraction pattern of this area, after floating and expanding (7) to the standard array size of 512 × 256; the reciprocal net and indexing of diffraction peaks for one of the two sides are indicated; (*c*) filtered image for this side, using the elliptical mask size in *b*; (*d*) cross-correlation map based on comparison of the central reference area indicated in *c* with the whole array; the peaks are at the best match positions, corresponding to the locations of the individual unit cells; (*e*) map of the magnitude (×20) and directions of deviations of the unit cells from the exact lattice positions; (*f*) residual deviations from the exact lattice positions after applying the corrections. The Fourier transform of the distortion-corrected image yielded the required values of amplitude and phase. To obtain data from the other side of the tube, the reciprocal net corresponding to that side was indexed in an equivalent way and the steps (*c–f*) repeated. Bar, 500 Å; scale of diffraction pattern, 1 cm = 0.0065 $Å^{-1}$.

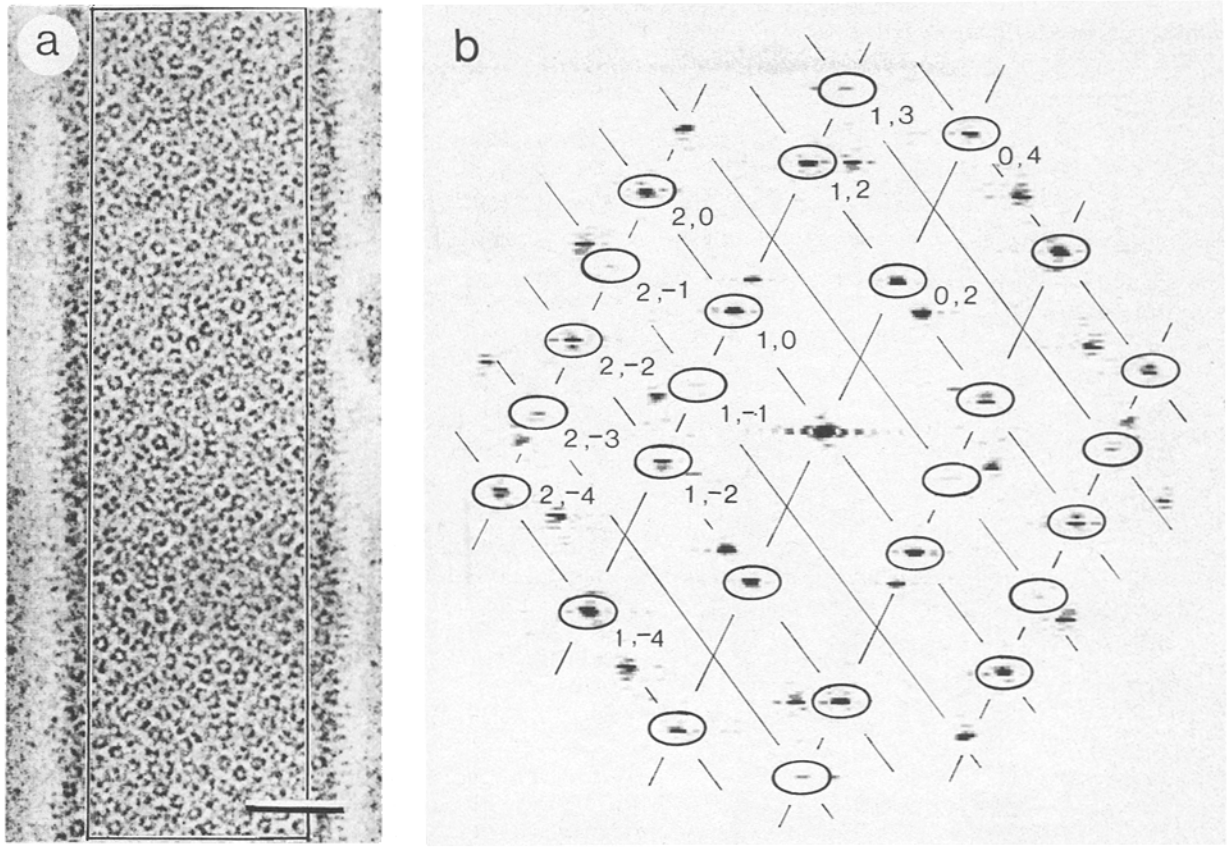
a
b
1,3
0,4
1,2
2,0
2,-1
0,2
1,0
2,-2
1,-1
2,-3
2,-4
1,-2
1,-4

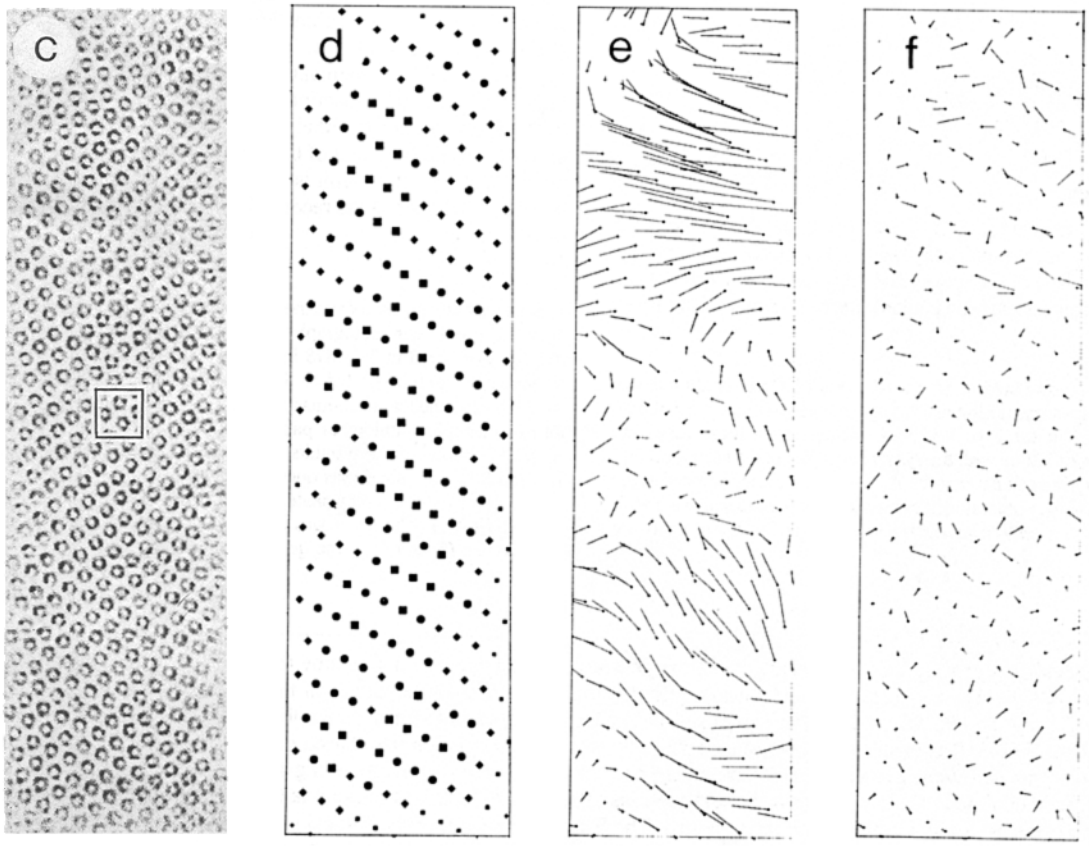
c
d
e
f

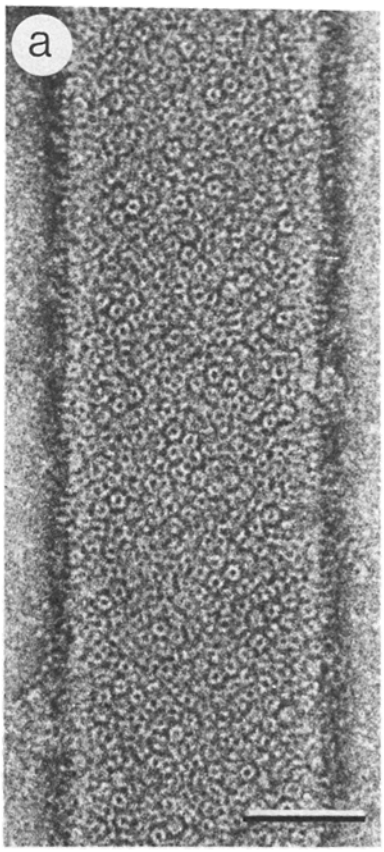
a

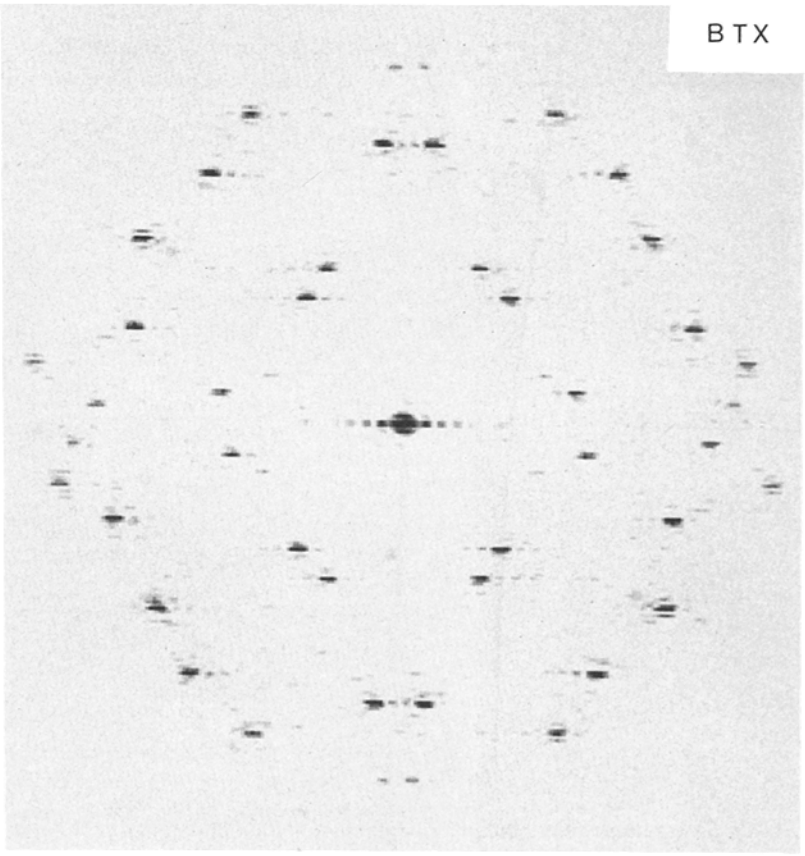
BTX

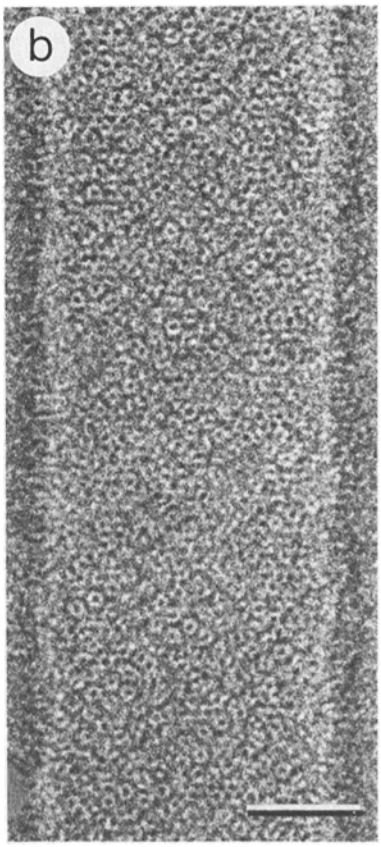
b

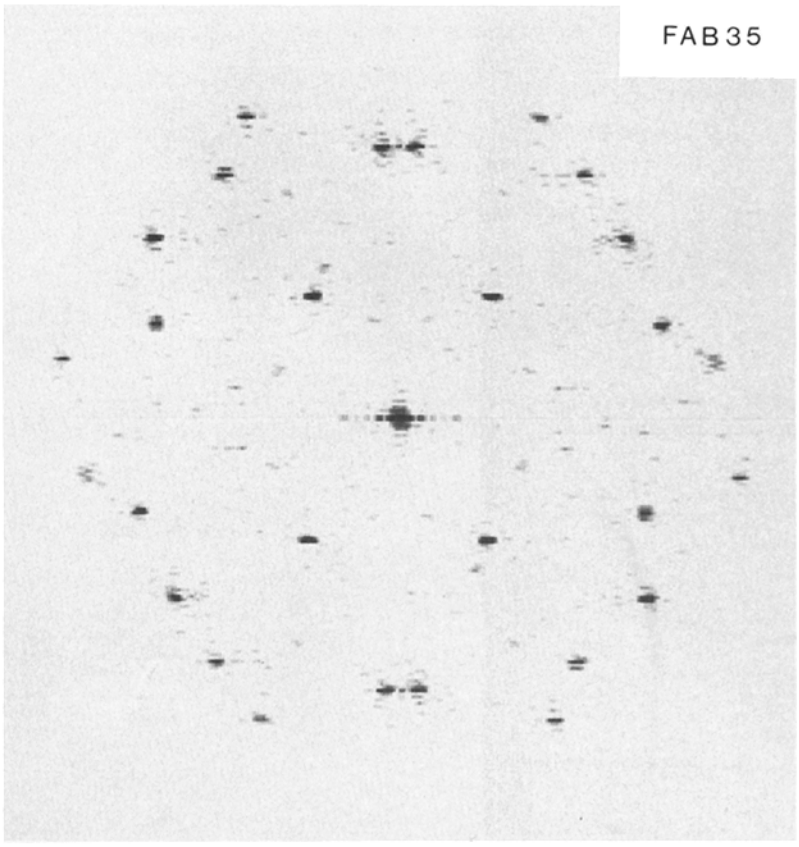
FAB35

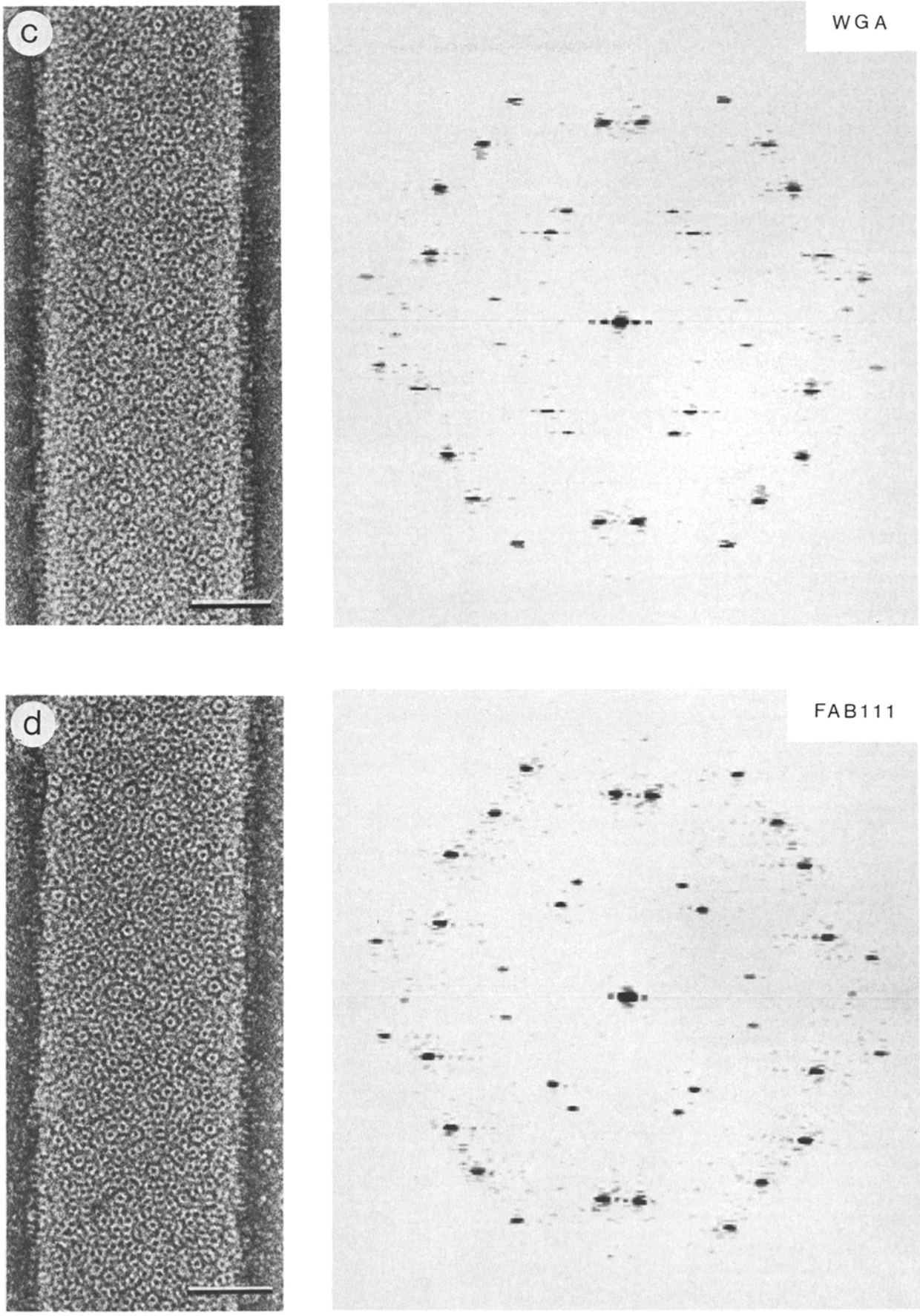

Figure 4. Images of tubes labeled with (*a*) BTX, (*b*) Fab35, (*c*) WGA, and (*d*) Fab111, and their corresponding computed diffraction patterns. Bar, 500 Å; scale of diffraction patterns, 1 cm = 0.0065 $Å^{-1}$.

cm^2 nitrocellulose, and then washed for three 10-min periods in quench buffer. Avidin-peroxidase (5 μg/ml) in quench buffer was added to the nitrocellulose sheet (vol ~8 ml/100 cm^2) and incubated for 1 h at room temperature. The nitrocellulose was washed for 30 min with several changes of PBS. The peroxidase substrate was freshly prepared and consisted of (*a*) 30 mg of α-chloro-napthol in 10 ml of cold methanol and (*b*) 30 μl of 30% H_2O_2 in 50 ml cold PBS. Parts *a* and *b* were mixed and added immediately to the nitrocellulose sheet. Development was stopped by pouring off the substrate and rinsing the sheet in PBS plus NaN_3. WGA binding was identified by the appearance of a dark purple band.

Antibody labeling of receptors, after SDS PAGE and electro-transfer to nitrocellulose (or diazophenylthioester paper), was as described (27). 1 ml of mAb111 (10 nM in quench buffer) was added to a strip of nitrocellulose (or diazophenylthioether paper) and incubated for 4 h at 22° ± 2°C. After washing, 1 nM ^{125}I-goat anti-rat IgG was added and incubated for 2 h. After a final washing, the paper strips were then autoradiographed for 6 h on preflashed (1) Kodak XAR film.

The SDS gels of receptors purified from the incubated vesicles (Fig. 2, lanes *1* and *2*) are similar to those of receptors purified from fresh electric organ, and show that all four polypeptides remain predominantly intact, despite the long incubation period. The δ-subunits of receptors from the incubated vesicles are also predominantly disulphide-bonded into dimers, as in the fresh tissue (Fig. 2, lanes *2* and *4* [5]). The nitrocellulose blots (Fig. 2, lanes *3–5*) demonstrate specificity of the mAb111 for the β-subunit and specificity of WGA for carbohydrate on the δ-subunit, as found for *Torpedo californica* (24). Specificity of mAb35 for the α-subunit has been demonstrated (30).

Electron microscopy

Samples in 5-μl aliquots were applied to freshly glow-discharged carbon support grids, washed with ~1 mg/ml cytochrome *c*, and negatively stained with 2% sodium phosphotungstate, pH 7.2. The labeling reagents were reacted with the tubes by application to the grids after the cytochrome *c* wash at the following concentrations: 4 μM for BTX, 1 μM for Fab35 and Fab111, and 10 μM (in the presence of 0.1 mM $CaCl_2$) for WGA. Reaction times ranged between 10 and 30 min. Prolonged application of WGA caused disordering of the crystals, rendering them unsuitable for further analysis. Fab111 was the only reagent used that bound to the cytoplasmic portion of the receptor, and hence to the inside of the tubes (3, 28); the accessibility of these sites may have been facilitated by the presence of holes at or near the extremities of many of the tubes.

The specimens were examined at 100 kV within 1–2 d of preparing the grids, using a Philips EM400 electron microscope equipped with a low dose kit. Micrographs were recorded at a magnification of 33,000 and a total dose of <10 electrons/Å^2. The Kodak S0163 film was developed in undiluted D19 developer for 10 min. To minimize variability between images, defocus values were required to be in the range of 12,000–16,000 Å, estimated from the positions in the optical diffraction patterns of Thon rings (29).

Analysis of Images

Criteria for selection of suitable images, the digitizing and Fourier transformation of appropriate areas, were as described (reference 3; Fig. 3). Additional computations used procedures for correcting distortions of the crystal lattice (12). The reciprocal nets corresponding to each of the two superimposed layers were identified (Fig. 3 *b*) and refined by a least squares fit to the coordinates of all the strong peaks. Filtered images corresponding to the separate sides were calculated from these nets (Fig. 3 *c*). The relative positions of the individual unit cells in each filtered image were determined by cross-correlation of a central reference area with the whole array (Fig. 3 *d*). Measurement of the deviations of the unit cells from a perfect lattice provided the vectors describing the distortions present (Fig. 3 *e*). Fourier transforms of the original images, after correction to minimize these distortions (Fig. 3 *f*), generated sharp diffraction peaks for the side being evaluated, and yielded accurate values for their integrated amplitude and phase. Comparison of distortion-corrected and uncorrected datasets indicated that the corrections were important in minimizing variability between images, and consequently in increasing the reliability of detection of small differences (see below).

The phases and amplitudes collected for each side of each tube were incorporated into averaged datasets as detailed in Table II, except for those cases where the phase errors, refined to a centrosymmetric origin, were >15°, or where diffraction peaks originating from the two sides overlapped. All images processed were of comparable size and quality to those in Fig. 4, and were scaled to yield the same total amplitude before being averaged.

A series of statistical tests were conducted on numerical maps calculated by Fourier synthesis of the data from the individual images. We divided the 23-image native dataset (Table II) into 11- and 12-image subsets (chosen at random), synthesized the maps for each image, and calculated on a point-by-point basis the mean density values and the standard deviation for each subset. In either case, the standard deviations were greatest at the centers of the receptors and at the symmetry axes, being ~2 and ~1.5 times larger in these regions than elsewhere. We showed, by applying the Student's *t* test (see also reference 23), that there were no significant differences between the two means at any point in the unit cell. In another test, the subsets were divided according to whether the images were of the side of the tube facing toward or away from the carbon support film. In this case, there were significant differences between the two means (at the 2% level) at two places within the unit cell. Hence, we concluded that the staining pattern is slightly dependent on the "sidedness" of the image and, to avoid any bias from this source, included approximately equal numbers of datasets from both sides in all of the averages (Table III).

Fourier and Statistical Difference Maps

To identify the positions of the ligands in the crystal lattice, Fourier syntheses were conducted of the difference terms: $F_l(h,k) - F_n(h,k)$, where $F_l(h,k)$ and $F_n(h,k)$ are the averaged Fourier terms (Table III) obtained for the ligand-bound and native structures, respectively. Data were scaled such that $\Sigma|F_l(h,k)| = \Sigma|F_n(h,k)|$; minor adjustments of the relative scales to account for the additional mass of the ligand did not affect the positions of the major difference peaks.

We applied statistical tests, as above, to evaluate the differences between the ligand-bound and native structures, and found in all cases, peaks where the difference between the two means were highly significant (<0.1% level). These peaks, located within the positive areas of the difference maps, were used to estimate the precise positions on the receptor of the ligand binding sites. We believe that this statistical analysis provides the best quantitative method to interpret the Fourier difference maps since it takes account of "noise" due, for example, to variability in the staining or floppiness of the ligand about its site of attachment. In support of this view, the statistical estimates for the BTX (or Fab35) binding sites on the α-subunits yielded only two probable locations per receptor and these locations, to a good approximation, were equivalent in relation to the overall structure (see below).

Results

Labeling Reagents

Described below are the results of experiments to localize the subunits, using receptor probes of molecular mass ranging between 8 and 50 kD, large enough to be resolved by electron crystallographic methods (see Table I). The smallest probe, BTX, attaches to the acetylcholine binding site on the extracellular surface of the α-subunit near cysteines 192 and 193 (16, 26, 34). A probe of intermediate size, WGA, is specific for *N*-acetylglucosamine residues on the δ-subunit of *T. californica* (24) and is also specific for this subunit of *T. marmorata* (Fig. 2). The largest probes, Fab35 and Fab111 (Fab fragments of monoclonal antibodies), bind to the main immunogenic region on the α-subunit between amino acid

Table II. Details of Averaged Datasets

Label applied	Number of images*	No. of molecules‡	Average phase error§
Native	23	11,000	7.0
BTX (α)	14	6,900	7.9
Fab35 (α)	10	5,200	9.9
Fab111 (β)	15	7,200	10.1
WGA (δ)	17	8,700	8.5

* No. of sides of tubes analyzed.
‡ Total No. of molecules included in average.
§ Based on comparison of individual phases with nearest centrosymmetric values.

Table III. Average Fourier Terms ($|F|$, Amplitude and Φ, Phase) for Native and Labeled Tubes

		Native		BTX		Fab35		WGA		Fab111	
h	*k*	$\|F\|$	Φ	$\|F\|$	Φ	$\|F\|$	Φ	$\|F\|$	Φ	$\|F\|$	Φ
0	5	6 (2.3)*	0	10 (2.9)	0	6 (3.0)	0	14 (4.9)	0	6 (2.6)	0
0	4	86 (7.7)	180	88 (10.1)	180	85 (10.7)	180	88 (9.2)	180	84 (13.0)	180
0	3	11 (5.1)	180	13 (4.4)	180	32 (11.1)	180	17 (4.0)	180	15 (8.4)	180
0	2	91 (12.3)	180	80 (10.7)	180	33 (13.4)	180	86 (15.8)	180	75 (8.1)	180
0	1	3 (2.4)	0	–	–	3 (2.0)	0	4 (9.4)	180	3 (2.5)	180
1	−4	129 (11.6)	0	134 (16.8)	0	129 (19.0)	0	133 (14.8)	0	169 (6.0)	0
1	−3	–	–	2 (0.9)	180	5 (2.3)	180	–	–	–	–
1	−2	70 (9.8)	0	70 (13.5)	0	23 (11.5)	0	57 (11.2)	0	62 (10.7)	0
1	−1	25 (6.3)	0	11 (7.4)	0	40 (11.3)	0	19 (7.2)	0	8 (6.0)	0
1	0	119 (14.0)	180	115 (9.8)	180	142 (14.8)	180	118 (11.6)	180	97 (11.5)	180
1	1	–	–	–	–	25 (5.9)	0	–	–	–	–
1	2	135 (11.4)	180	154 (13.9)	180	173 (13.2)	180	153 (15.0)	180	169 (6.1)	180
1	3	29 (6.4)	180	31 (8.3)	180	12 (6.1)	180	23 (5.9)	180	23 (5.5)	180
2	−4	70 (8.9)	180	74 (10.1)	180	76 (9.5)	180	73 (11.4)	180	85 (11.2)	180
2	−3	51 (8.6)	180	45 (5.3)	180	33 (10.2)	180	44 (11.2)	180	27 (4.8)	180
2	−2	115 (12.4)	0	116 (14.8)	0	134 (6.2)	0	127 (11.0)	0	132 (14.2)	0
2	−1	25 (9.1)	0	17 (5.0)	0	12 (5.2)	0	9 (3.6)	0	8 (9.1)	0
2	0	114 (6.6)	180	117 (8.8)	180	114 (9.2)	180	115 (10.6)	180	120 (9.0)	180
3	−2	9 (2.9)	180	10 (3.1)	180	7 (1.8)	180	11 (4.0)	180	7 (1.6)	180

* Figures in parentheses are standard deviations.

residues 46–127 (27) and to a cytoplasmic site on the β-subunit between residues 360–410, respectively (27, 28). Several other cytoplasmic subunit-specific Fabs were tried, but were less effective, possibly because their antigenic determinants were made inaccessible by the crystal packing or were shielded by cytoskeletal proteins (9).

Binding Sites

Examples of the native and labeled tubes and their diffraction patterns are given in Figs. 3 and 4. A sufficient number of tubes were selected and analyzed in each case to provide the average structures from more than 5,000 molecules (Table II). All averaged datasets were comparable in terms of phase errors (Table II) and resolution (Table III). Difference maps calculated from the labeled minus the native datasets were used to locate the ligand within the crystal lattice, and statistical maps calculating the *t* distribution (see Materials and Methods) were used to obtain best estimates for the site of attachment of the ligand on the receptor. These maps refer to the crystal lattice as viewed from the outside of the tube, that is, from the synaptic side of the membrane (3).

The apparent occupancy of each ligand was estimated roughly by assuming that the strength of the difference peak would be in proportion to its molecular weight and that the stain-exposed portion of the receptor seen in projection would represent about three-quarters of its total mass (4). Values obtained were: ~25% (WGA; Fab111), ~50% (α_2 site, Fab35), and ~75% (α_1 site Fab35; α_1 and α_2 sites, BTX).

α-BTX (α). BTX had a minor effect on the appearance of the tubes and their diffraction patterns (compare Figs. 3 *a* and 4 *a*). This is to be expected because BTX contributes to the unit cell only ~6% of its total mass. The Fourier difference map (Fig. 5 *a*, top) displays rather broad peaks, giving only an approximate estimate for the location of this ligand in the crystal lattice. Within these broad peaks, however, there are just two points where the differences due to the added mass are of high significance (<0.1% level; Fig. 5 *a*, middle). These points correspond to the most probable positions of the ligand binding sites (α_1 and α_2) on the projected structure (Fig. 5 *a*, bottom). The sites lie directly over the subunits at distances of 27 Å (α_1) and 28 Å (α_2) from the central axis of the receptor. Their angular separation is 142°. Because of the crystal symmetry, the α-subunits of neighboring molecules are juxtaposed; thus the distances between the α_1-subunits of adjacent receptors (42 Å), or between the α_2-subunits of adjacent receptors (36 Å), is smaller than the distance between the α_1- and α_2-subunits of a single molecule (53 Å).

Fab35 (α). Fab35 had a more noticeable effect on the appearance of the tubes and produced pronounced changes in some of the diffraction peaks (e.g., the 0, 2 peaks, Fig. 4 *b*; Table III). The Fourier difference map identified two possible locations for this ligand per molecule. The statistical map (Fig. 5 *b*, middle) indicated that the most probable positions for the binding sites are at the side of the receptor at radii of 31 Å (α_1) and 39 Å (α_2), and separated by an angle of 146°. These Fab35 sites are each ~45° anticlockwise from the sites identified above.

WGA (δ). WGA labeling of the δ-subunits yielded one major peak in the Fourier difference map (Fig. 5 *c*, top) and a corresponding pair of peaks in the statistical difference map (Fig. 5 *c*, middle). This pair of peaks identifies sites in close proximity on either side of a dyad axis (Fig. 5 *c*, bottom). The short distance between these two sites (24 Å) is comparable to the dimensions of WGA, and could account for the tendency of this molecule to disorder the crystal lattice (see Materials and Methods).

Fab111 (β). Fab111 labeling of the β-subunit led to identification of a site between the pair of α-subunits (Fig. 5 *d*). The significant differences are spread over a larger portion of the receptor than in the other examples, possibly because

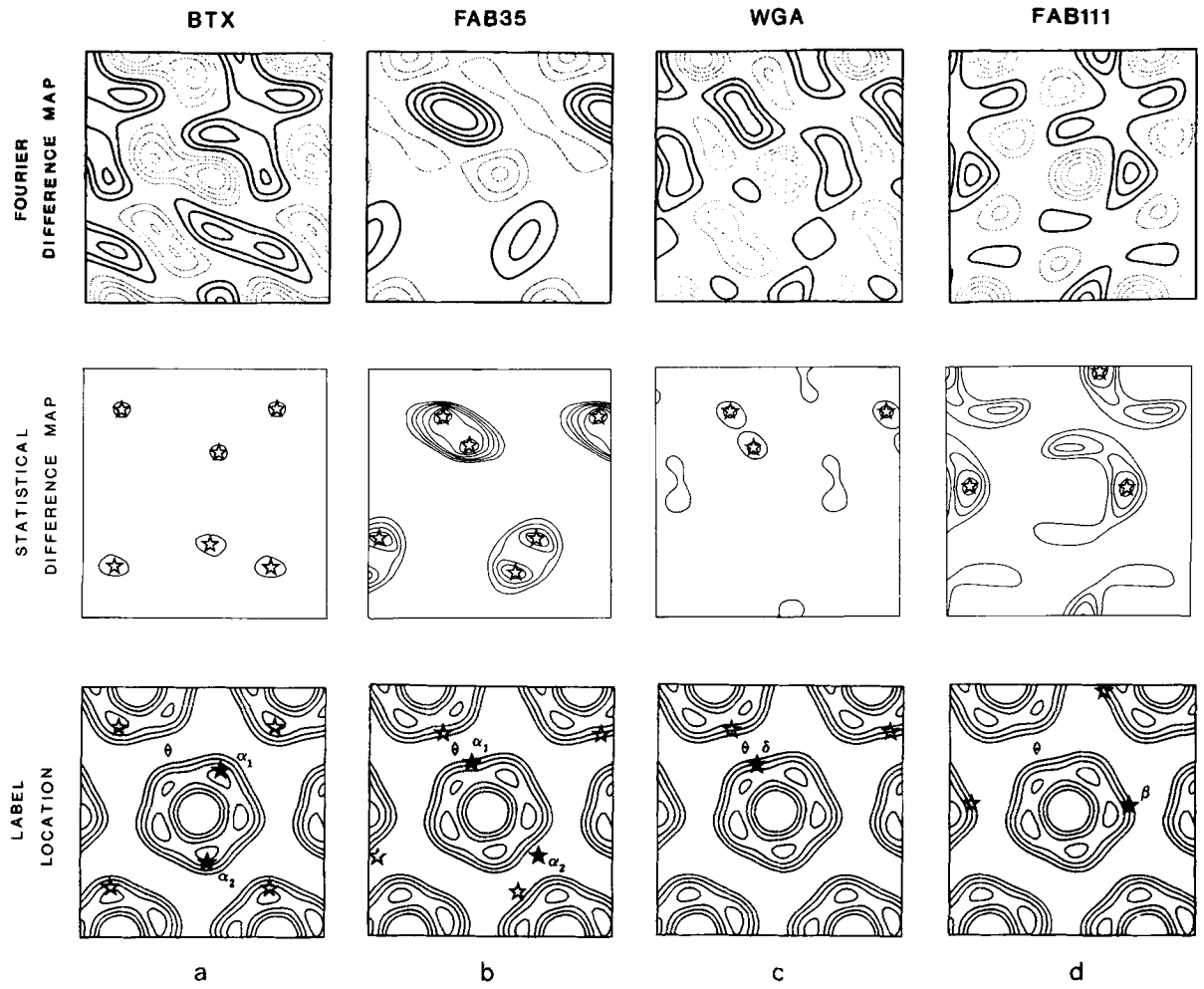

Figure 5. Identification of binding sites of (*a*) BTX, (*b*) Fab35, (*c*) WGA, and (*d*) Fabl11 on the receptor, as viewed from the synaptic side of the membrane. The Fourier difference maps (*top*) show positive (continuous contours) and negative (dotted contours) peaks, corresponding respectively, to exclusion of the stain (i.e., presence of ligand) and accumulation of the stain; the zero level contour has been omitted. The statistical difference maps (*middle*) show contours of increasing t values (see Materials and Methods); the outermost contours enclose regions where the probability that the differences are real and not due to chance is >99.9%; stars over the highest t values identify the ligand binding sites. The projection maps (*bottom*; from reference 4) show the positions of the binding sites with respect to individual receptors in the crystal lattice; the sites associated with central receptor are emphasized; the dyad symbol (θ) relates the pair of receptors tentatively identified previously (3) as the δ-subunit–linked dimer.

this probe is trapped inside the tubes between two crystalline arrays of receptors and therefore is constrained to lie in only one or two orientations.

The remaining subunit, the γ-subunit, must lie between locations determined for δ and α_2 since this is the only region unaffected by any of the above probes.

Discussion

Earlier analyses of the tubular crystals showed that the five subunits of the receptor are arranged symmetrically around the channel, having their axes approximately perpendicular to the membrane plane (3, 4). However, with the exception of a tentative assignment for the δ-subunit, the identities of the individual subunits remained unclear. In this study, four subunit-specific labels have been used to identify the subunits and explore their arrangement around the channel. First, the α-subunits were located on the basis of the differences in mass obtained by exposing the crystals to BTX. The differences were highly significant at two points only, making it unlikely that they were due to changes in receptor structure, which would have more extensive effects. Fab35 labeling of the α-subunits confirmed these assignments by binding at two points each ~45° anticlockwise from the BTX-binding sites (a distance sufficient to account for the fact that both ligands can bind to the receptor simultaneously [30]). The observed angular separation of the BTX and of the Fab35 positions (142° and 146°) confirmed that the α-subunits are not adjacent to one another (2, 8, 14, 35), but separated by an intervening subunit. Second, the δ-subunit was located on the basis of the differences obtained by exposing to WGA. WGA bound in the region where neighboring subunits come closest together, consistent with the finding that the δ-subunits are disulphide-linked (Fig. 2). Third, the

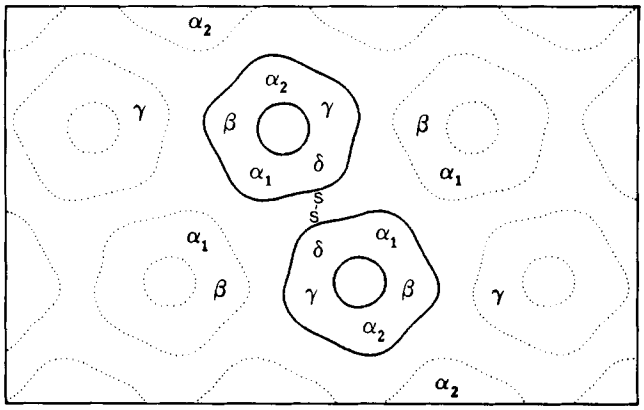

Figure 6. The arrangement of the subunits around the receptor and the disulphide-linked dimer, determined by the labeling experiments. Receptors are oriented in the crystal lattice so that the α-subunits of neighboring molecules are juxtaposed. The ribbons of paired receptors seen on the surfaces of vesicles during crystallization are formed by side-to-side packing of dimers (3) and probably therefore involve interaction between the β- and γ-subunits.

β-subunit was located on the basis of the differences obtained by exposing to FabIII. FabIII bound in the single-subunit region between the α-subunits, in agreement with the assignment deduced from cross-linking experiments (11). It was not necessary to develop a probe for the γ-subunit, since its position had to be the only unassigned location remaining.

The reliability of these assignments is reinforced by consistency between alternative lines of evidence. Each α-subunit has been identified twice, using probes that are quite distinct in terms of size, shape, and specificity. The δ-subunit has been localized to a position that is the same as that deduced from the crystal packing (3). This position is also the only candidate remaining that would entail direct apposition of chemically equivalent regions on neighboring molecules. The β- and γ-positions have not been assessed by alternative means and would be wrongly assigned if the subunits were azimuthally misaligned by a large amount on either side of the membrane (since FabIII is a cytoplasmic probe whereas the others are extracellular). However, this seems most unlikely in view of the structural evidence (4) that the subunits are untilted in their passage through the bilayer.

Fig. 6 shows the organization of the subunits within the receptor, the dimer and the crystal lattice, according to these results. It is a property of the crystal symmetry that individual receptors are oriented so that not only the δ-subunits but also the α-subunits of neighboring molecules are closely juxtaposed. A tendency for receptors to associate in the membranes through their α-subunits has been noted in fluorescent energy transfer studies (15). Contacts between the β- and γ-subunits appear to be responsible for the ribbons formed by side-to-side packing of dimers, which are observed on the surfaces of vesicles during the early stages of crystallization (3). Since ribbons of identical morphology are also observed in intact postsynaptic membranes immediately after isolation (13), the intermolecular contacts shown in Fig. 6 are quite possibly the same as those generally present at the synapse.

Two sites on the extracellular surface of the α-subunit appear to have been localized, in projection: the acetylcholine binding site (using BTX) and the main immunogenic region (using Fab35). Since the receptor has pseudo-pentagonal structural symmetry (4), one would expect equivalent sites on the two α-subunits to be at about the same radii and ∼2 × 360/5 = 144° apart. The estimates for the acetylcholine binding sites (radii, 27 and 28 Å; included angle, 142°) are in excellent accord with this symmetry. The corresponding estimates for the main immunogenic region (31 and 39 Å; 146°) are also in good agreement, considering that the localization errors are greater in this case due to the larger probe size. The three-dimensional disposition of these sites has not been revealed directly. However, quantitative structural determinations have shown that the extracellular portion of the receptor is a tubular structure, ∼60-Å long, and having a pentagonal cross section like that in Fig. 6 (4). The acetylcholine-binding site projects well within the molecular boundary formed by this structure (Fig. 5 *a*) and therefore almost certainly lies at the (synaptic) end of the subunit, a result also deduced from x-ray diffraction measurements (18). In contrast, the Fab35 site projects almost exactly onto the external molecular boundary of the receptor (Fig. 5 *b*), suggesting that the main immunogenic region is at (or close to) the side of the subunit, between the synaptic end and the surface of the membrane.

The positions of the main immunogenic regions on opposite faces of the receptor may account for the fact that antibodies like mAb35 cannot bind simultaneously to both α-subunits of a single molecule, yet are very effective at cross-linking molecules to each other (6). Receptor–receptor cross-linking by antibodies to the main immunogenic region is pathologically important (32) since it triggers antigenic modulation, which causes receptor loss, in the autoimmune disease myasthenia gravis (33).

This crystallographic study to localize ligand-binding sites on the receptor has yielded more precise information than has been obtainable by electron microscopy of isolated molecules or dimers, and more direct information than has been obtainable by cross-linking experiments. We have demonstrated that the receptors, embedded in native membranes, show little sign of biochemical degradation. The state of structural preservation has been evaluated by objective methods, and the significance of the differences contributed by the ligands has been established statistically from large numbers of molecules. The arrangement we have found for the subunits is consistent with that deduced from cross-linking experiments. (11).

We are most grateful to Richard Henderson for the computer programs used to correct for lattice distortions. We thank our colleagues for helpful discussions.

This research was supported by grants to N. Unwin from the National Institutes of Health (GM-27764, GM-30387) and to J. Lindstrom from the National Institutes of Health (NS-11323), the Muscular Dystrophy Association, the Alexander S. Onassis Public Benefit Foundation, the U.S. Army (DAMD17-86-C-6148), and the Los Angeles and California Chapters of the Myasthenia Gravis Foundation.

Received for publication 23 February 1987, and in revised form 30 March 1987.

References

1. Bonner, W., and R. Laskey. 1974. A film detection method for tritium-labelled proteins and nucleic acids in polyacrylamide gels. *Eur. J. Biochem.* 46:83–88.

2. Bon, F., E. Lebrun, J. Gomel, R. V. Van Rapenbusch, J. Cartaud, J.-L. Popot, and J.-P. Changeux. 1984. Image analysis of the heavy form of the acetylcholine receptor from *Torpedo marmorata*. *J. Mol. Biol.* 176: 205–207.
3. Brisson, A., and P. N. T. Unwin. 1984. Tubular crystals of acetylcholine receptor. *J. Cell Biol.* 99:1201–1211.
4. Brisson, A., and P. N. T. Unwin. 1985. Quaternary structure of the acetylcholine receptor. *Nature (Lond.)*. 315:474–477.
5. Chang, H. W., and E. Bock. 1977. Molecular forms of acetylcholine receptor. Effects of calcium ions and a sulfhydryl reagent on the occurence of oligomers. *Biochemistry*. 16:4513–4520.
6. Conti-Tronconi, B., S. Tzartos, and J. Lindstrom. 1981. Monoclonal antibodies as probes of acetylcholine receptor structure. 2. Binding to native receptor. *Biochemistry*. 20:2181–2191.
7. DeRosier, D. J., and P. B. Moore. 1970. Reconstruction of the three-dimensional images from electron micrographs of structures with helical symmetry. *J. Mol. Biol.* 52:355–369.
8. Fairclough, R. H., J. Finer-Moore, R. A. Love, D. Kristofferson, P. J. Desmeules, and R. M. Stroud. 1983. Subunit organization and structure of an acetylcholine receptor. *Cold Spring Harbor Symp. Quant. Biol.* 48: 9–20.
9. Froehner, S. C. 1986. The role of the postsynaptic cytoskeleton in AChR organization. *Trends Neurosci.* 9:37–41.
10. Gullick, W. J., and J. M. Lindstrom. 1983. Mapping the binding of monoclonal antibodies to the acetylcholine receptor from *Torpedo californica*. *Biochemistry*. 22:3312–3320.
11. Hamilton, S. L., D. R. Pratt, and D. C. Eaton. 1985. Arrangment of the subunits of the nicotinic acetylcholine receptor of *Torpedo californica* as determined by α-neurotoxin cross-linking. *Biochemistry*. 24:2210–2219.
12. Henderson, R., J. M. Baldwin, K. H. Downing, J. Lepault, and E. Zemlin. 1986. Structure of purple membrane from *Halobacterium halobium*: recording, measurement and evaluation of electron micrographs at 3.5Å resolution. *Ultramicroscopy*. 19:147–178.
13. Heuser, J. E., and S. R. Salpeter. 1979. Organization of acetylcholine receptors in quick-frozen, deep-etched, and rotary-replicated *Torpedo* postsynaptic membrane. *J. Cell Biol.* 82:150–173.
14. Holtzman, E., D. Wise, J. Hall, and A. Karlin. 1982. Electron microscopy of complexes of isolated acetylcholine receptor, biotinyl-toxin, and avidin. *Proc. Natl. Acad. Sci. USA*. 79:310–314.
15. Johnson, D. A., J. G. Voet, and P. Taylor. 1984. Fluorescence energy transfer between cobra α-toxin and molecules bound to the acetylcholine receptor. *J. Biol. Chem.* 259:5715–5725.
16. Kao, P. N., A. J. Dwork, R. J. Kaldany, M. L. Silver, J. Wideman, S. Stein, and A. Karlin. 1984. Identification of the α-subunit half-cysteine specifically labelled by an affinity reagent for the acetylcholine receptor binding site. *J. Biol. Chem.* 259:11662–11665.
17. Karlin, A., E. Holtzman, N. Yodh, P. Lobel, J. Wall, and J. Hainfield. 1983. The arrangement of the subunits of the acetylcholine receptor of *Torpedo californica*. *J. Biol. Chem.* 258:6678–6681.
18. Kistler, J., R. M. Stroud, M. W. Klymkowsky, R. A. Lalancette, and R. H. Fairclough. 1982. Structure and function of an acetylcholine receptor. *Biophys. J.* 37:371–383.
19. Lindstrom, J., B. Einarson, and S. Tzartos. 1981. Production and assay of antibodies to acetylcholine receptors. *Methods Enzymol.* 74:432–460.
20. Lindstrom, J., B. Gullick, B. Conti-Tronconi, and M. Ellisman. 1980. Proteolytic nicking of the acetylcholine receptor. *Biochemistry*. 19:4791–4795.
21. Mage, M. 1980. Preparation of Fab fragments from IgG's of different animal species. *Methods Enzymol.* 70:142–150.
22. McCarthy, M. T., J. P. Earnest, E. T. Young, S. Choe, and R. M. Stroud. 1986. Molecular neurobiology of the acetylcholine receptor. *Annu. Rev. Neurosci.* 9:383–413.
23. Milligan, R. A., and P. F. Flicker. 1987. Structural relationship of actin, myosin and tropomyosin revealed by cryo-electron microscopy. *J. Cell Biol.* 105:9–18.
24. Nomoto, J., N. Takehashi, Y. Nagaki, S. Endo, Y. Arata, and K. Hayashi. 1986. Carbohydrate structures of acetylcholine receptor from *Torpedo californica* and distribution of oligosaccharide among the subunits. *Eur. J. Biochem.* 157:233–242.
25. Popot, J.-L., and J.-P. Changeux. 1984. The nicotinic receptor of acetylcholine: structure of an oligomeric integral membrane protein. *Physiol. Rev.* 64:1162–1239.
26. Ralston, S., V. Sarin, H. L. Thanh, J. Rivier, J. L. Fox, and J. Lindstrom. 1987. Synthetic peptides used to locate the α-bungarotoxin binding site and immunogenic regions on α subunits of the nicotinic acetylcholine receptor. *Biochemistry*. In press.
27. Ratnam, M., P. B. Sargent, V. Sarin, J. L. Fox, D. Le Nguyen, J. Rivier, M. Criado, and J. Lindstrom. 1986. Location of antigenic determinants on primary sequences of subunits of nicotinic acetylcholine receptor by peptide mapping. *Biochemistry*. 25:2621–2632.
28. Ratnam, M., D. Le Nguyen, J. Rivier, P. B. Sargent, and J. Lindstrom. 1986. Transmembrane topography of nicotinic acetylcholine receptor: immunological tests contradict theoretical predictions based on hydrophobicity profiles. *Biochemistry*. 25:2633–2643.
29. Thon, F. 1966. Zur Defokussierungsabhaengigkeit des Phasenkontrastes bei der elekronenmikroskopischen Abbildung. *Z. Naturforsch.* 21a: 476–478.
30. Tzartos, S. J., D. E. Rand, B. L. Einarson, and J. Lindstrom. 1981. Mapping of surface structures of *Electrophorus* acetylcholine receptor using monoclonal antibodies. *J. Biol. Chem.* 256:8635–8645.
31. Tzartos, S. J., L. Langeberg, S. Hochschwender, L. W. Swanson, and J. Lindstrom. 1986. Characteristics of monoclonal antibodies to denatured *Torpedo* and to native calf acetylcholine receptors: species, subunit and region specificity. *J. Neuroimmunol.* 10:235–253.
32. Tzartos, S. J., M. E. Seybold, and J. Lindstrom. 1982. Specificities of antibodies to acetylcholine receptors in sera from myasthenia gravis patients measured by monoclonal antibodies. *Proc. Natl. Acad. Sci. USA*. 79: 188–192.
33. Tzartos, S. J., D. Sophianos, and A. Efthimiadis. 1985. Role of the main immunogenic region of acetylcholine receptor in myasthenia gravis. An Fab monoclonal antibody protects against antigenic modulation by human sera. *J. Immunol.* 134:2343–2349.
34. Wilson, P., T. Lentz, and E. Hawrot. 1985. Determination of the primary amino acid sequence specifying the α-bungarotoxin on the α-subunit of the acetylcholine receptor from *Torpedo californica*. *Proc. Natl. Acad. Sci. USA*. 82:8790–8794.
35. Zingsheim, H. P., F. J. Barrantes, F. Frank, W. Hanicke, and D. C. Neugebauer. 1982. Direct structural localization of two toxin-recognition sites on an ACh receptor protein. *Nature (Lond.)*. 299:81–84.